

Modeling the Performance of the Standard Cirrus Glider using Navier-Stokes CFD

Thomas Hansen
thhh@kth.se

Royal Institute of Technology,
100 44 Stockholm, Sweden



Abstract

In this report the performance of the Standard Cirrus glider is simulated using a computational fluid dynamics (CFD) code. The computations are performed by solving the incompressible Navier-Stokes equations considering the flow field as steady. To calculate the transitional boundary layer flow a correlation based transition model is used. It is found that the numerical model is able to predict the performance of the Standard Cirrus glider well. The simulations using the transition model are found to improve the results compared to the fully turbulent simulations, except for the region of the stall.

1. Introduction

The development of modern computer tools has led to a revolution for the design and construction of high performance gliders. Today, the aerodynamic and the structural potential of new designs can be investigated and refined using computers to produce gliders with performance and handling qualities inconceivable just a few decades ago. Gliders like the JS1, ASG29 and the Diana 2 are examples of the improvements possible when applying the latest computer tools in combination with experience and experimental testing. Glide ratios of about 1:50 and maximum speed above 280 km/h are today normal for the modern glider having 15 and 18 m of wing span. However, the new numerical tools stand in sharp contrast to the methods applied for the design of the first high performance gliders. Some 30 years ago the tools available consisted almost entirely of analytic approximation methods, wind tunnel experiments and flight testing. The materials and the accuracy of the production methods available at the time was also a limiting factor in the quest to develop high performance gliders.

In this report the Standard Cirrus glider is simulated by solving the Reynolds-Averaged Navier-Stokes (RANS) equations in the commercial CFD software STAR CCM+ [1]. The main purpose for the work is to create a validated reference model for the performance of the glider in steady level flight. To predict the important boundary layer flows the correlation based transition model named the $\gamma - Re_\theta$ transition model [2] is used and its accuracy is investigated in detail. The results obtained in this report should enable future investigations regarding possible performance and handling quality enhancements for the glider. The design of new winglets, the installation of an electrical engine and research on new turbulator technology are examples of studies that could benefit from using a validated RANS model. The model of the Standard Cirrus is also intended to be a reference model for investigating other numerical

simulation tools. The abilities and limitations of less computational expensive codes such as lifting line methods, vortex-lattice codes and potential flow solvers can all be evaluated better by comparing the results to the validated Navier-Stokes model.

To perform the simulations, the geometry of the specific Standard Cirrus named LN-GTH is first measured using a digitizing arm and a surface model is created. Then the performance of the airfoil used at the outer part of the Cirrus wing is investigated using a two dimensional mesh. The simulations are performed to investigate the accuracy of the $\gamma - Re_\theta$ transition model in detail. The two dimensional computations are validated by comparing the results to experimental values from the low-turbulence pressure wind tunnel at Langley, NASA. Finally, the three dimensional model of the Standard Cirrus is simulated in steady level flight for velocities from 90 km/h to 160 km/h. The three dimensional CFD simulations are validated by comparing the results to recent flight tests performed for the Standard Cirrus at Idaflieg, Germany.

2. The Standard Cirrus



The Standard Cirrus was designed by Dipl. Ing. Klaus Holighaus at the Schempp-Hirth factory and flew for the first time in March 1969. The glider is a 15 m design without flap and was originally built to compete in the standard class. The glider uses an all moving tailplane, is equipped with air brakes on the upper side of the wings, and can carry 80 kg of water ballast to increase the flight performance. In Figure 1 the Standard Cirrus glider is shown. The wing of



Figure 1: The Standard Cirrus glider.

the glider is designed using two different airfoils. The root airfoil blends linearly into the airfoil that is used at the outer part of the wing. The outer wing airfoil is constant from the start of the aileron to the tip of the wing. The best glide ratio for the glider is about 1:37 and the maximum speed is 220 km/h. The glider is known for its good handling qualities, large cockpit and ability to climb well in turbulent thermals. The Standard Cirrus is today considered to be one of the best gliders for participating in club class competitions.

3. Method



In the following the methods used to perform the simulations of the Standard Cirrus are given. First, the approach used to perform the measurements of the glider is explained. Then the methodology used to investigate the performance of the Standard Cirrus in both two and three dimensions is presented.

3.1. Measurements of the glider geometry

To perform a qualitative analysis of the flight performance for the Standard Cirrus the 'as built' geometry is measured on a specific Standard Cirrus named LN-GTH. To reproduce the glider geometry, the airfoil on both the wing, elevator and rudder is measured using a digitizing arm [3]. The wing is measured at the root, start of the aileron and at the tip of the wing. Tail section measurements are performed at the largest and smallest chord respectively. By fixing stainless steel shims to the surface of the wing and tail at the measurement stations a straight edge is created and used to guide the digitizing arm. In Figure 2 the digitizing arm is depicted. The digitizing arm is operated in combination with a surface CAD tool [4] and about



Figure 2: Microscribe digitizing arm.

200 points are captured for each measurement. To increase the accuracy, five measurement series are taken for each airfoil geometry. The final splines of the airfoils are created in a two dimensional panel code [5] using the averaged measured data. The chord lengths and the thickness of the trailing edge of the wing and tail are also measured using a digital caliper gauge [6]. All other measurements of the glider, such as the position of the wing to fuselage fairing, height of the tail, etc., are taken using a hand held laser [7]. The factory drawings are used as reference. The fuselage, however, is designed by modifying a CAD model which has been used to perform a similar CFD simulation of the Standard Cirrus using the TAU code at the German Aerospace Center (DLR) [8].

3.2. Navier Stokes solver

The simulations of the Standard Cirrus are performed by using the parallelized flow solver STAR CCM+. The code uses a cell centered finite volume discretization approach that can be

applied to cells of arbitrary polyhedral shapes. The program is designed to take on all aspects of the CFD process and tools enabling both CAD design and post-processing of the results are implemented. The meshing technology is automated and is capable of creating both a tetrahedral, polyhedral and trimmed hexahedral mesh in a Cartesian based coordinate system. A wide range of turbulence models are implemented, including the $k - \omega$ SST turbulence model of Menter [9] which is a prerequisite for the $\gamma - Re_\theta$ transition model [1]. To solve the RANS equation for the simulations of the Standard Cirrus the segregated solver in STAR CCM+ is used. The flow field is modeled using a constant density model and the air is considered to be steady and incompressible. The turbulent flow is modeled with the $k - \omega$ SST turbulence model, and the transitional boundary layer flow is simulated using the $\gamma - Re_\theta$ transition model. All simulations are performed on a Dell power blade cluster running 36 CPU's in parallel.

3.3. The $\gamma - Re_\theta$ transition model

The laminar-turbulent transition process is important when predicting the performance of gliders. For Reynolds numbers below 3 million, this transition process often takes the form of a laminar separation bubble. When this occurs, the separating laminar layer is followed by turbulent reattachment, just behind a recirculation region. In Figure 3 an illustration of the transition process on the upper side of an airfoil is shown. For the simulations of the Standard

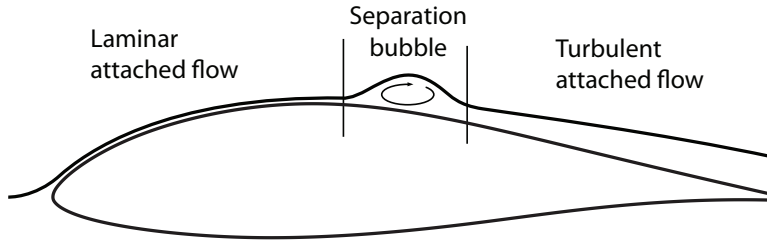


Figure 3: Laminar separation bubble.

Cirrus the transition process is modeled using the $\gamma - Re_\theta$ transition model. This is a correlation-based transition model that solves two extra transport equations, one for intermittency, γ , and one for the local transition onset momentum thickness Reynolds number, Re_{θ_t} . The model relates the local momentum thickness Reynolds number, Re_θ , to the critical value, Re_{θ_c} , and switches on the intermittency production when Re_θ is larger than the local critical value. The only input the model requires is the definition of the Re_{θ_t} correlation defined in the free-stream. This definition ensures that the Re_{θ_t} correlation takes the value of 1 in the free-stream, and 0 inside the boundary layer [1]. The mesh requirements for using the $\gamma - Re_\theta$ transition model is a high quality, refined low Reynolds number mesh. The distance from the wall boundary to the first cell centroid in the mesh determines how the boundary layer is resolved by the turbulence model. This distance is defined by the y^+ value

$$y^+ = \frac{yu^*}{\nu} , \tag{1}$$

where y is the normal distance from the wall to the wall-centroid, u^* is the reference velocity and ν is the kinematic viscosity. To enable the $\gamma - Re_\theta$ transition model to converge, the y^+ values need to be in the region 0.1 to 1, and have a growth rate and stream-wise mesh spacing in the transition area fine enough to capture the laminar separation bubble [10]. By performing

the simulations as fully turbulent, the transition process is ignored and only turbulent air-flow is present in the boundary layer.

3.4. Two dimensional calculations

To investigate the accuracy of the $\gamma - Re_\theta$ transition model, the performance of the airfoil used on the outer part of the Standard Cirrus wing is investigated in two dimensions. The simulations are validated by comparing the results to experimental data from the low-turbulence pressure wind tunnel at Langley, NASA [11]. The airfoil geometry used for the simulations is also obtained from the NASA experiment performed in 1977, and is believed to be measurements from a Standard Cirrus wing. Hence, the performance of the newly refinished LN-GTH airfoil can be compared to the NASA measurements of the airfoil from 1977. To determine the required quality of the mesh when using the $\gamma - Re_\theta$ transition model a mesh dependency study is performed. The interesting angles of attack, α , are calculated using an O-mesh. The O-mesh is constructed with a hyperbolic extrusion method using a structured mesh tool [12]. To create a pressure outlet boundary the downstream far-field edge is cut at 40 to 110 degrees. Upstream, a velocity inlet boundary is used. In Figure 4 an example of the O-mesh is shown. To reproduce the flow condition at the test section from the NASA wind tunnel experiment, the

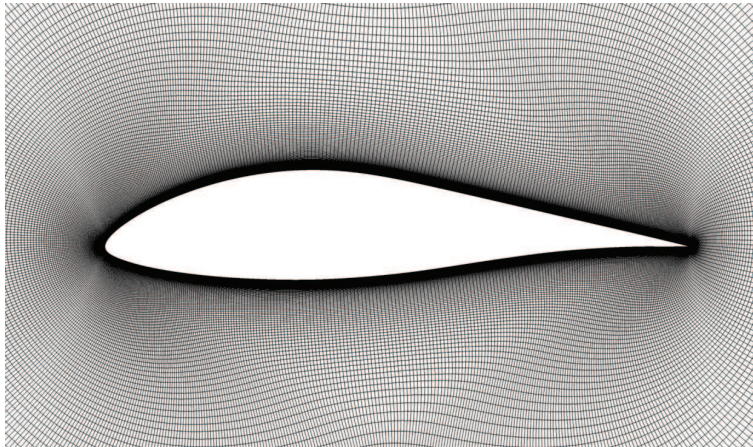


Figure 4: Hyperbolic extruded O-mesh.

turbulent intensity and turbulent viscosity ratio is used. The value for the turbulent intensity is found from [13] to be 0.02 % and a turbulent viscosity ratio of 10 is used to imitate external flow conditions. The correct values applied to the inlet boundary are calculated using the turbulence decay laws from the $k - \omega$ SST turbulence model [1]. All simulations are performed for the Reynolds number of 1.5 million. Java scripts and stopping conditions are used to execute the simulations. For all residuals, a drop in accuracy to the fourth decimal is used as stopping criterion. In addition, an asymptotic stopping criterion for the monitored coefficients, C_l and C_d is used ensuring a bounded accuracy on the fifth decimal for the last 50 iterations. For all calculations the free-stream edge definition for the $\gamma - Re_\theta$ model is arbitrary put at 5 mm from the airfoil surface. Fully turbulent simulations are also performed and used as reference to the transition model investigations. The mesh criteria for the fully turbulent simulations are taken from previous work performed on wind turbine blades [14]. The results from the two dimensional simulations are also compared to calculations performed using the panel codes Xfoil [15] and Rfoil [16].

3.5. Three dimensional calculations

In steady level flight the lift produced by an aircraft needs to equal the weight. For a glider this situation occurs at a steady, unaccelerated descent, where θ is the equilibrium descent glide angle. The lift force on coefficient form is given by

$$C_L = \frac{L}{q_\infty S} = \frac{mg}{q_\infty S} , \quad (2)$$

and the drag coefficient is given by

$$C_D = \frac{D}{q_\infty S} . \quad (3)$$

Here, m is the mass of the glider, g is the gravitational constant and S is the reference area. The dynamic pressure q_∞ is denoted

$$q_\infty = \frac{1}{2} \rho_\infty V_\infty^2 , \quad (4)$$

where ρ_∞ is the density of air and V_∞ is the free-stream velocity. Since the change in Reynolds number due to difference in density at different altitudes are small, the descent glide angle θ can be found from

$$\tan(\theta) = \frac{1}{C_L/C_D} . \quad (5)$$

Hence, the descent glide angle θ is only a function of the lift-to-drag ratio, C_L/C_D , and does not depend on altitude or wing loading. However, to achieve a given C_L/C_D at a given altitude, the glider must fly at a specific velocity V_∞ called the equilibrium glide velocity. The value of V_∞ is dependent on both altitude and wing loading [17].

To evaluate the performance of the Standard Cirrus the speed polar is calculated. The speed polar for the glider is a measure of the gliders performance. The polar shows the rate of sink at different free-stream velocities and is found from

$$h = V_\infty \sin(\theta) . \quad (6)$$

To validate the three dimensional simulations the speed polar is compared to flight measurements performed for the Standard Cirrus at Idaflieg. The flight data from Idaflieg are provided as calibrated air speed (CAS) using $\rho_0 = 1.225 \text{ kg/m}^3$ as reference density, and the simulations are therefore also performed using this density. The Standard Cirrus used for the flight tests at Idaflieg has a mass of 355.6 kg and a reference area of 10 m². The simulations are performed for velocities between 90 km/h and 160 km/h, as these are the steady level flight velocities normally used. At lower velocities, the glider should be circling in thermals, and not be in steady level flight. At higher velocities the increase in sink rate deteriorates the performance of the glider, and should be avoided during normal flight.

To simulate the performance of the Standard Cirrus, two CFD models are constructed and calculated. One model is created to simulate the lift and drag coefficients of the wing and fuselage, where the wing, the wing fairing and the fuselage is included. To find the correct angles of attack, that produce the needed lift coefficient at the specific velocities, two simulations at different angles of attack are performed. The linearity of the lift slope for the Standard Cirrus is then used to find the angle of attack that produces the correct lift coefficient. Another model is created to calculate the drag coefficient of the tail section. This model is constructed with both the tail section and the fuselage present, and have the elevator positioned at zero degree angle

of attack. To account for Reynolds number effects the drag coefficient of the tail is simulated for all investigated velocities. An isotropic, trimmed hexahedral mesh is created for the two models using CCM+. To reduce the number of cells in the mesh, symmetry conditions are applied. Hence, only half the glider is present in the models. The required quality for the three dimensional mesh when using the $\gamma - Re_{\theta}$ transition model is investigated in a mesh dependency study. The boundary layer is constructed using a 20 layer, 30 mm thick hyperbolic extruded prism layer. The mesh outside the prism layer has a growth rate of 1.1. In Figure 5 the wing and fuselage mesh is shown. The outer boundary of the flow domain is constructed as

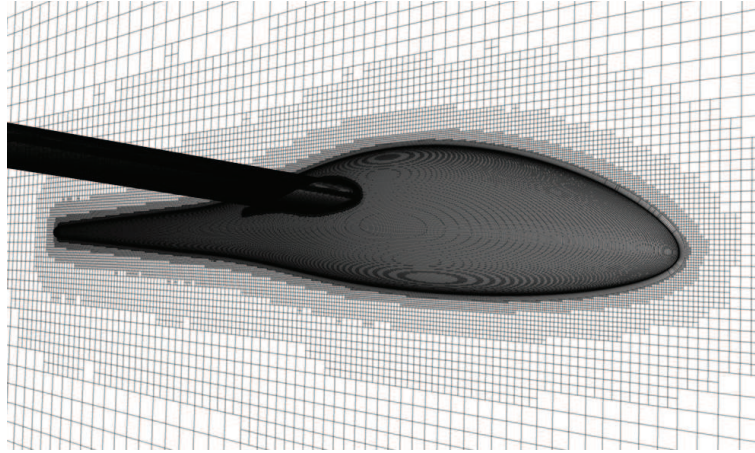


Figure 5: Trimmed hexahedral mesh.

a half-sphere, and is positioned 50 m from the wall boundary of the glider surface. The domain is split and has a velocity inlet and pressure outlet boundary upstream and downstream of the glider, respectively. A turbulence intensity of 0.1% and a turbulent viscosity ratio of 10, initiated at the inlet boundary is applied to specify the turbulence in the air-flow for all simulations. Java scripts and stopping conditions are also used to execute the three dimensional simulations. The stopping criteria for the residuals is set to ensure a drop in accuracy to the third decimal. The asymptotic stopping criterion for the monitored coefficients, C_l and C_d is to be asymptotic bounded on the fourth decimal for the last 50 iterations. The free-stream edge definition for the $\gamma - Re_{\theta}$ model is put at 5 mm from the glider surface. Fully turbulent simulations are also performed and used as reference to the transition model investigations. To better investigate the difference between the two CFD methodologies the mesh used for the fully turbulent simulations are the same as for the calculations performed with the $\gamma - Re_{\theta}$ transition model.

4. Results

In the following, the results from the investigations of the Standard Cirrus glider are presented. First, the measurement of the airfoil geometry from the outer wing of the LN-GTH glider is shown and compared to the original coordinates. Then the results from the two and three dimensional simulations are given.

4.1. Geometry measurement results

The airfoil used at the outer part of the Standard Cirrus wing is found in [19] to be the FX 66-17 All-182. This airfoil is designed by Dr. F.X. Wortmann at the University of Stuttgart

and the original coordinates are obtained from the Stuttgart airfoil catalog [20]. To investigate the quality of the airfoil on LN-GTH, comparison to both the original airfoil coordinates and to the measurements obtained from the NASA experiment are performed. In Figure 6 the airfoil comparison is shown. The figure is scaled to better visualize the differences between the airfoils. As seen in the figure the three airfoils do not match exactly. The difference between the original

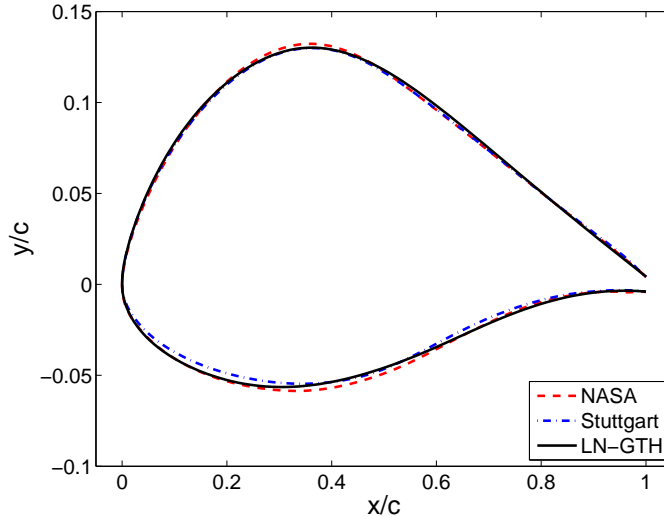


Figure 6: Comparison of Standard Cirrus outer wing airfoil.

Stuttgart coordinates and the NASA measurements are discussed in [11] and is believed to be due to the fiberglass construction techniques available at the time of production. The airfoil geometry from the LN-GTH measurements can be seen to fit the NASA airfoil better than the Stuttgart coordinates. The largest difference between the LN-GTH and the NASA airfoil is found at the thickest part of the airfoil geometry. This difference is believed to be from refinishing the gelcoat on the 34 year old LN-GTH glider.

4.2. Two dimensional results

The O-mesh with the smallest number of cells that enables the $\gamma - Re_\theta$ model to converge is found from the mesh dependency study. This mesh has 600 cells wrapped around the airfoil, a growth rate of 1.05 and y^+ values below 1 for all simulated angles of attack. By reducing the number of cells on the airfoil it is found that the range of angles of attack possible to be simulated, is also reduced. In Figure 7 the results for the lift and drag coefficient from the two dimensional investigations are given. To the left in the figure the lift coefficient vs. the angle of attack is shown. Here, the predictions from the CFD simulations using the transition model can be seen to compare well to the experimental data. The results using the transition model predict the lift coefficient equally well as the panel codes Xfoil and Rfoil for the angles of attack between -5 and 5 degrees. For higher angles of attack the transition model compares better to the experimental data than the results from the panel codes. However, the transition model is unable to simulate the occurrence of the stall and a too high lift coefficient is predicted in this region. The fully turbulent CFD model can be seen to underestimate the lift coefficient for all positive angles of attack. This is because the pressure around the airfoil is wrongly calculated since no laminar air-flow is present in the model [14]. Interestingly, the Rfoil calculations can be seen to capture the occurrence of the stall better than the Xfoil simulations. To the right in the figure the lift coefficient C_l vs. the drag coefficient C_d is shown. Here the predictions from the

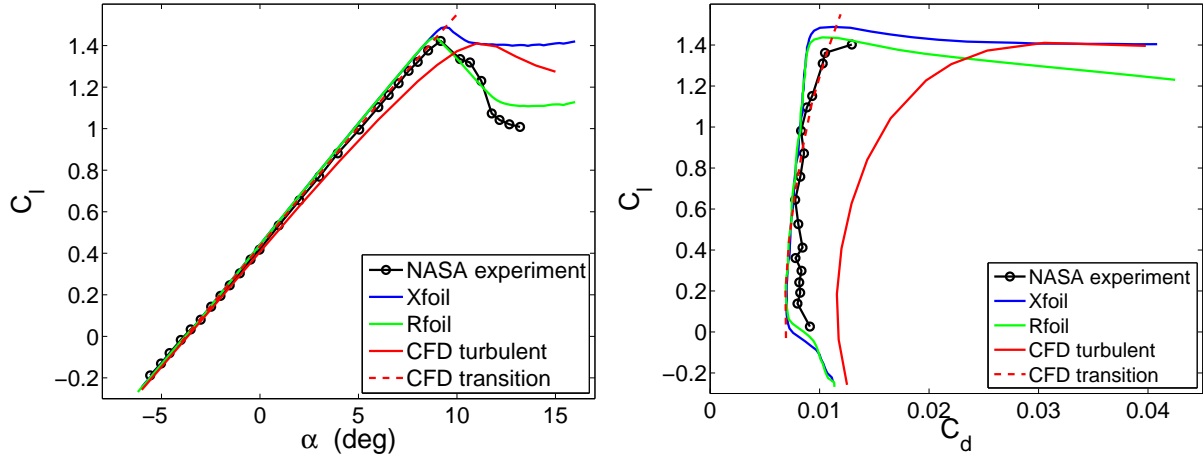


Figure 7: Airfoil performance comparison

CFD simulations using the transition model can be seen to compare well to the experimental data. The transition model performs equally well to the panel codes for the C_l values from 0 to 0.6. For higher C_l values, the transition model compares better to the experimental data than Xfoil and Rfoil. The fully turbulent CFD model can be seen to over predict the drag coefficient heavily for all values of C_l . By not accounting for the laminar air-flow in the boundary layer the viscous drag for the airfoil is wrongly calculated. In Figure 8 the results for the position of the transition are given. As can be seen in the figure the position of the laminar separation bubble

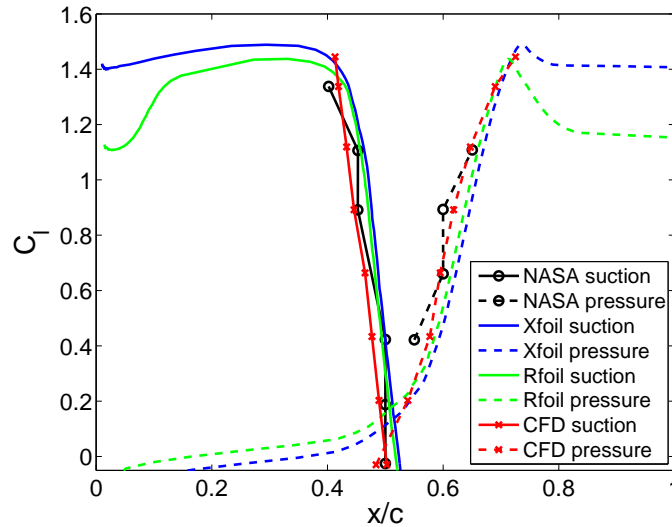


Figure 8: Position of the laminar separation bubble.

using the $\gamma - Re_\theta$ transition model compare well to the experimental data. The prediction using the Xfoil and Rfoil codes can be seen to be slightly further back on the airfoil for both the suction and pressure side. This is believed to be due to the difference in the methods used to calculate the transition process. The panel codes predict the transition position at the end of the laminar separation bubble [15], while the $\gamma - Re_\theta$ model is able to predict the start position of the laminar transition bubble. Finally, a comparison of the lift-to-drag ratio for the NASA airfoil measured in 1977 and the LN-GTH airfoil is depicted in Figure 9. The results are obtained using the Rfoil code and indicate a slightly better performance for the LN-GTH airfoil at angles of attack below 8 degrees for the investigated flow condition.

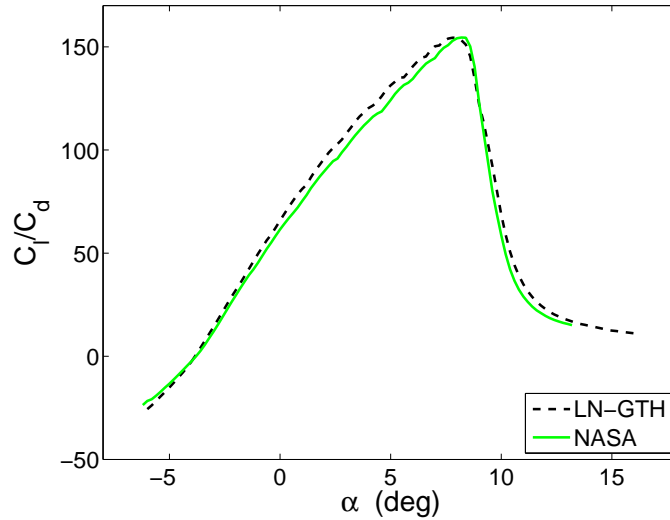


Figure 9: Lift-to-drag ratio for two measured Standard Cirrus airfoil geometries.

4.3. Three dimensional results

In Figure 10 the production of turbulent kinetic energy on the top side of the Standard Cirrus is visualized. The transition model is able to predict the transition from laminar to turbulent air-flow on both the wings and the fuselage of the glider. To the left in the figure a free-stream velocity of 95 km/h is simulated. At this velocity the transition process starts approximately

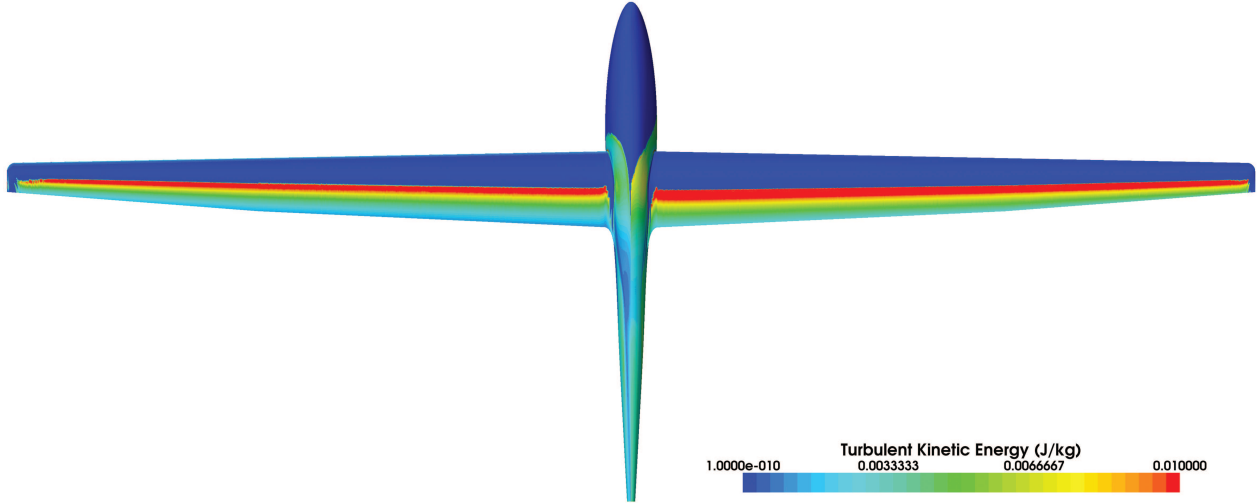


Figure 10: Top side transition, left 95 km/h, right 160 km/h.

at the mid-chord along the span of the wing. The laminar separation bubble can be seen as the region where the production of turbulent kinetic energy is the highest. Behind the laminar separation bubble the reattachment region is seen, followed by turbulent attached air-flow. To the right in the figure a 160 km/h simulation is depicted. At this velocity the position of the laminar separation bubble is moved slightly backwards compared to the 95 km/h simulation. The production of turbulent kinetic energy is also increased, hence, a larger laminar separation bubble is produced. In Figure 11 the production of turbulent kinetic energy on the bottom side of the Standard Cirrus is shown. The transition from laminar to turbulent

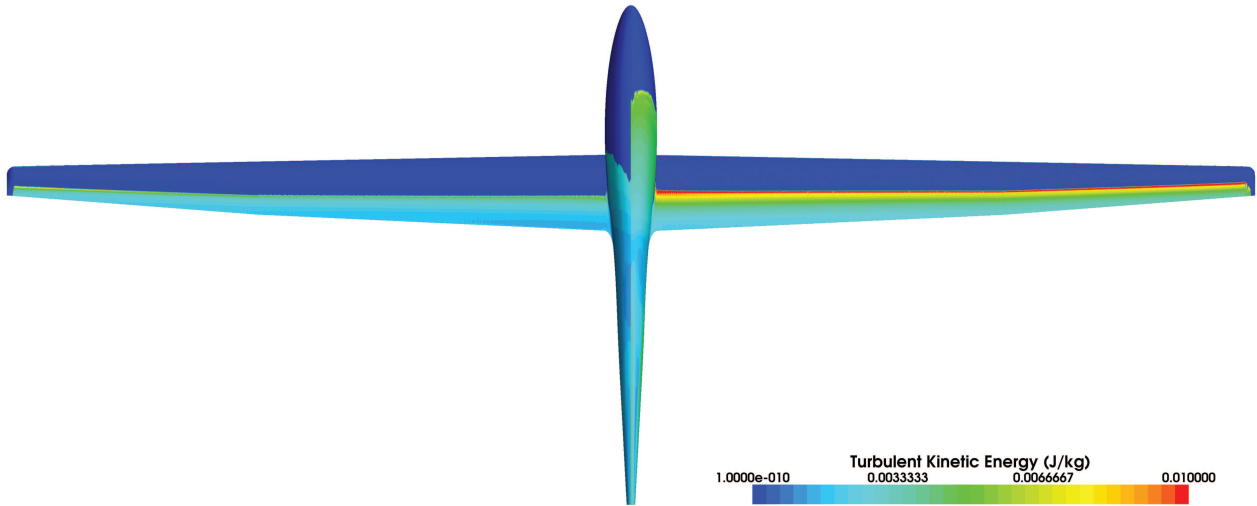


Figure 11: Bottom side transition, left 95 km/h, right 160 km/h.

air-flow on the bottom side is positioned slightly behind the middle chord along the span of the wing for 95 km/h (left in figure). The production of turbulent kinetic energy is low and the laminar separation bubble on the bottom side of the wing is small. The position of the laminar separation bubble for 160 km/h (right in figure) is moved slightly forward compared to the 95 km/h simulation. The production of turbulent kinetic energy is also larger for this simulated velocity, hence a more defined laminar separation bubble is produced. At the tip of the wings and at the wing to fuselage fairing the $\gamma - Re_\theta$ transition model predicts large regions of laminar flow. This scenario is not believed to model the real flow conditions correctly. The highly rotated flow produced by the tip vortex and at the wing to fuselage region is believed to be outside the capabilities of the $\gamma - Re_\theta$ model.

The production of turbulent kinetic energy on the fuselage of the Standard Cirrus is visualized in Figure 12. In the top figure the transition position for the 95 km/h simulation is

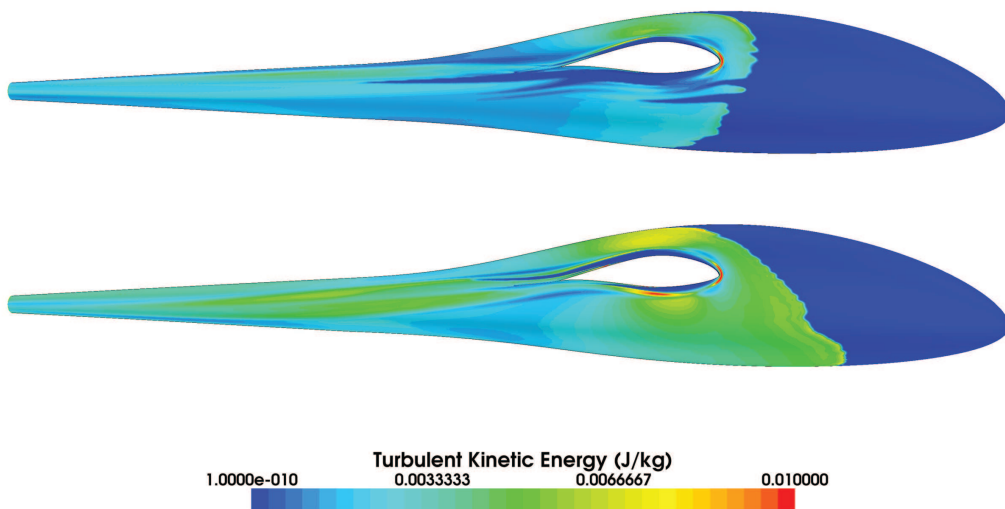


Figure 12: Fuselage transition, top 95 km/h, bottom 160 km/h.

shown. Here, the transition from laminar to turbulent can be seen to be close to the start of the wing-fuselage fairing. In the bottom figure the production of turbulent kinetic energy for the 160 km/h simulation is shown. Due to the higher velocity and lower angle of attack the transition has moved forward. More turbulent kinetic energy is especially produced at the lower part of the fuselage. Both the fuselage shape, the angle of attack and the velocity thus determines the position of the transition process. In the 95 km/h simulation a large region of laminar flow can be seen on the bottom side of the wing-fuselage fairing and for the 160 km/h simulation a region of laminar flow can be seen on the upper side of the wing-fuselage fairing. These laminar regions are believed to be incorrect, and to be a result of positive pressure gradients created due to the inflow angles. It is also known that sailplane cockpit ventilation is affected by internal flow resistance within the fuselage, causing air to escape between the canopy frame and the cockpit edge. This air leakage trips the laminar boundary layer on the canopy and fuselage to turbulent air-flow and increases the profile drag for the fuselage [18]. However, the position of the main boundary layer transition line for the different simulations are found to compare well to measurements found in [19].

In Figure 13 the production of turbulent kinetic energy on the top of the elevator section is shown. Again, the trends from the simulations performed for the wings of the glider can be observed. The 95 km/h simulation to the left in the figure has a low production of turbulent kinetic energy making the laminar separation bubble small. The position of the transition for the 160 km/h simulation to the right in the figure is moved forward and the production of turbulent kinetic energy has increased. Also on the elevator surface large regions of laminar flow exist at the tips.

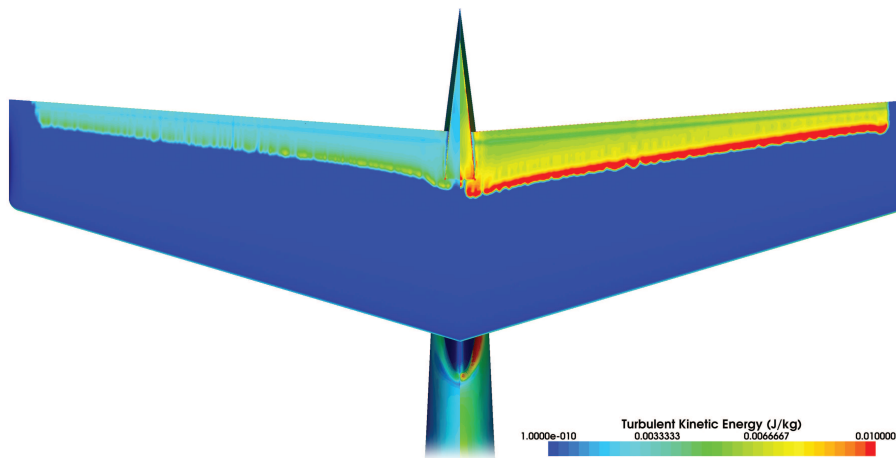


Figure 13: Elevator transition, left 95 km/h, right 160 km/h.

The production of turbulent kinetic energy on the lower side of the elevator and the tail section of the Standard Cirrus is shown in Figure 14. To the left in the figure the result from the 95 km/h simulation is depicted and to the right the 160 km/h simulation is visualized. It can be seen that the presence of the fuselage has a large impact on the production of turbulent kinetic energy. The turbulent flow condition from the fuselage initiates the transition process almost on the leading edge for the lower part of the fin. The upper part of the fin experiences less turbulence and the transition occurs later. Also in the region where the elevator and fin are connected, the transition occurs closer to the leading edge. The drag coefficient of the tail section is found to be Reynolds number dependent and a reduction in C_d of about 10 % is found for the 160 km/h compared to the 95 km/h simulation.

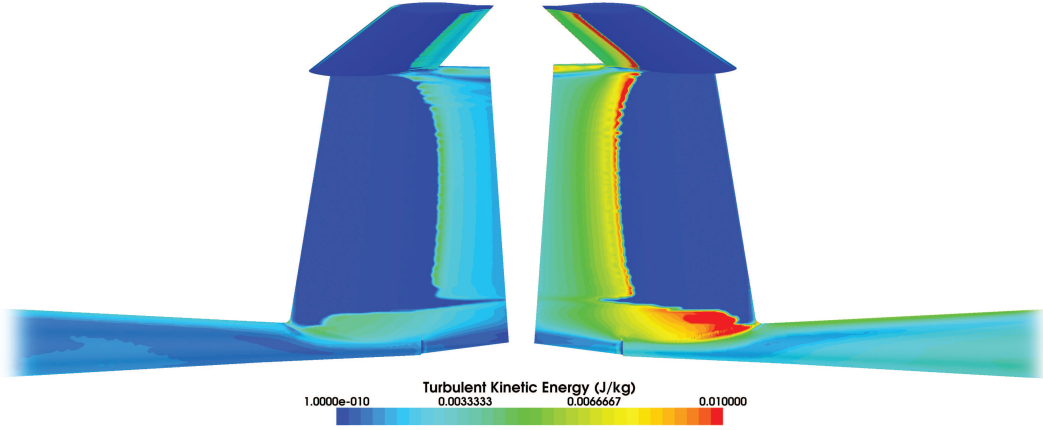


Figure 14: Tail section transition, left 95 km/h, right 160 km/h.

To obtain a converged solution for the simulations using the $\gamma - Re_\theta$ model, all calculated grids are adjusted to meet the mesh criteria for both the different velocities and angles of attack. Since the $y +$ value for the mesh scales with the velocity the grids at high velocities use a smaller distance to the first cell centroid. At high angles of attack, more cells on the wing of the glider are needed to obtain a converged solution. The number of cells in the mesh are thus increased from 28 million to 41.8 million cells for the 95 km/h to the 160 km/h simulation, respectively. The simulation of the fuselage and tail section are performed at zero degree angle of attack. Hence, only considerations for the $y +$ values are needed. The fuselage and tail mesh use about 7.8 million cells.

In Figure 15 the calculated speed polar for the Standard Cirrus is compared to flight measurements from Idaflieg. The simulations performed using the $\gamma - Re_\theta$ transition model can be seen to compare well to the real flight data. For velocities below 100 km/h the simulations are

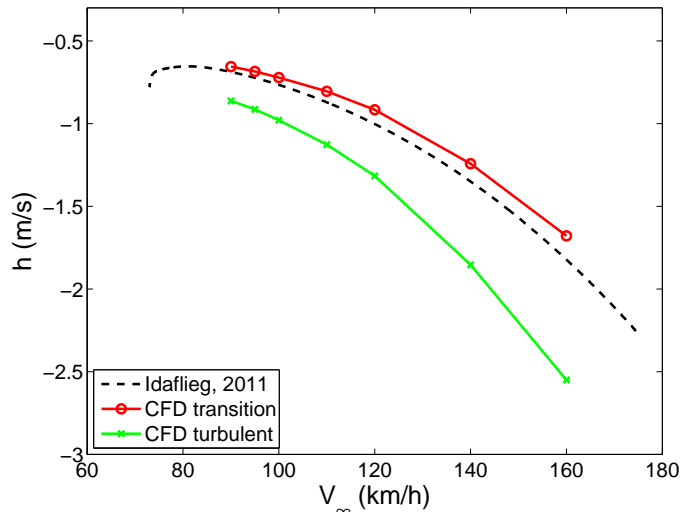


Figure 15: Standard Cirrus speed polar.

closely matched to the flight measurements. At higher velocities, the sinking speeds are slightly under predicted. The measured best glide ratio for the Standard Cirrus from the Idaflieg flight tests are found to be 36.51 at 94.47 km/h. For the simulations performed using the $\gamma - Re_\theta$ model the best glide ratio is found to be 38.51 at 95 km/h. The turbulent calculations of the

Standard Cirrus can be seen to heavily overestimate the drag and thus the sinking speeds. The difference between the simulated results and the flight measurements increase at higher flight speeds. This is due to an increase in profile drag from not having laminar flow present in the model. The best glide ratio for the fully turbulent simulations is found to be 28.96 at 90 km/h.

In Table 1 the angles of attack for the Standard Cirrus simulations are given. The zero angle of attack for the CFD models of the glider is referenced to the weighing position as found in the flight and service manual [21]. The higher angles of attack needed to produce the different lift coefficients when performing the simulations as fully turbulent compared to using the $\gamma - Re_\theta$ model are evident.

V_∞	[km/h]	90	95	100	110	120	140	160
C_L	[-]	0.911	0.818	0.738	0.610	0.512	0.376	0.288
$\alpha_{transition}$	[deg]	2.663	1.770	1.013	-0.207	-1.128	-2.396	-3.220
$\alpha_{turbulent}$	[deg]	3.265	2.274	1.472	0.169	-0.805	-2.133	-2.992

Table 1: Input data for CFD simulations.

5. Conclusions

In this report the performance of the Standard Cirrus glider is simulated using the computational fluid dynamics code STAR CCM+. The computations are performed by solving the incompressible Navier-Stokes equations and considers the flow field to be steady. The turbulent flow is modeled using the $k - \omega$ SST turbulence model and to model the transitional boundary layer flow the $\gamma - Re_\theta$ transition model is applied. To investigate the performance of the $\gamma - Re_\theta$ model, calculations are first performed using a two dimensional grid. The final three dimensional simulations of the Standard Cirrus glider are validated by comparing the results to recent flight measurements from Idaflieg.

It is found that the numerical model is able to predict the performance of the Standard Cirrus glider well. The simulations performed using the $\gamma - Re_\theta$ transition model improves the results for the lift and drag predictions compared to fully turbulent calculations for low angles of attack. For high angles of attack, i.e. stalled condition the $\gamma - Re_\theta$ transition model is unable to converge. The best glide ratio for the Standard Cirrus from the Idaflieg flight tests is measured to be 36.51 at 94.47 km/h. For the simulation using the $\gamma - Re_\theta$ transition model the best glide ratio is calculated to be 38.51 at 95 km/h. The fully turbulent simulations predict the best glide ratio for the glider to be 28.96 at 90 km/h. The large deviations in the prediction of the glide ratio when using fully turbulent simulations are caused by the absence of laminar air-flow in the boundary layer for the glider. By accounting for the interference drag from the cockpit edges, as well as the drag from the tail and wing tip skids, the results from the simulations using the $\gamma - Re_\theta$ transition model could be improved. Additionally, the drag of the tail is simulated using a simplified model where the elevator is positioned at zero angle of attack. By accounting for the extra drag due to the elevator deflection needed to sustain steady level flight, the result should be further improved. Future studies should investigate the drag production from the glider in more detail and focus on applying the $\gamma - Re_\theta$ transition model for high angles of attack.

References

- [1] CD-Adapco. *Introducing STAR-CCM+*. User guide, STAR-CCM+ version 6.04.016, 2011.
- [2] R.B. Langtry and F.R. Menter. *Transition Modeling for General CFD Applications in Aeronautics*. American Institute of Aeronautics and Astronautics. AIAA 2005-522.
- [3] GHOST 3D, LLC. *MicroScribe 3D digitizer product details*. <http://www.microscribe.ghost3d.com>, August 2011.
- [4] Rhinoceros, NURBS modeling for windows. CAD surface tool. www.rhino3d.com, September 2011.
- [5] XFLR5. *Analysis of foils and wings operating at low Reynolds numbers*, Guidelines for XFLR5 v6.03, February 2011.
- [6] PAV. Digital workshop caliper gauge 1000 mm. <http://www.pav.eu/products/>, December 2011.
- [7] Bosch. Handheld laser range finder DLE 50 professional. <http://www.bosch-pt.com/productspecials/professional/dle50/select/index.htm>, December 2011.
- [8] S. Melber-Wilkending, G. Schrauf, and M. Rakowitz. *Aerodynamic Analysis of Flows with Low Mach- and Reynolds-Number under Consideration and Forecast of Transition on the Example of a Glider*.
- [9] CFD Online. SST k-omega model. http://www.cfd-online.com/Wiki/SST_k-omega_model, December 2011.
- [10] P. Malan, *Calibrating the $\gamma - Re_\theta$ Transition Model for Commercial CFD*. American Institute of Aeronautics and Astronautics, 082407.
- [11] D. M. Somers *Expero and theoretical low-speed aerodynamic characteristics of a wortmann airfoil as manufactures on a fiberglass sailplane*, NASA TN 0-8324, February 1977.
- [12] Pointwise, Inc. Structured mesh tool. <http://www.pointwise.com/apps/airfoil.shtml>, December 2011.
- [13] A. E. von Doenhoff, and F. T. Abbot, jr. *The langley two-dimensional low-turbulence pressure tunnel*, NASA TN 1283, May 1947.
- [14] T. Hansen. *Wind turbine simulations using Navier-Stokes CFD*, Master thesis, KTH, July 2010.
- [15] M. Drela, and H. Youngren. *XFOIL 6.9 User Primer*. MIT, 2001. <http://web.mit.edu/drela/Public/web/xfoil/>, December 2011.
- [16] B.O.G. Montgomerie, A.J. Brand, J. Bosschers, and R.P.J.O.M. van Rooij. *Three-Dimensional effects in stall*. NREL. TUD, ECN-C-96-079, June 1997.
- [17] J. D. Anderson Jr. *Aircraft Performance and Design*. McGraw-Hill, Maryland, 1999.
- [18] Jonker sailplanes. <http://www.jonkersailplanes.co.za>, December 2011.
- [19] F. Thomas. *Fundamentals of Sailplane Design*. College Park Press, Maryland, 1999.
- [20] D. Althaus, and F. X. Wortmann *Stuttgart profile catalog I*. Institut für Aerodynamik und Gasdynamik, Stuttgart, 2011.
- [21] Shempp-Hirth Flugzeugbau GmbH. *Flight and service manual for the sailplane Standard Cirrus*, Kirchheim-Teck, 1969.